Injection-level-dependent internal quantum efficiency and lasing in low-defect GaN nanowires

John B. Schlager[a], Norman A. Sanford, Kris A. Bertness, and Alexana Roshko

National Institute of Standards and Technology, Boulder, Colorado 80305, USA

(Received 14 October 2010; accepted 4 January 2011; published online 28 February 2011)

INTRODUCTION top

Growing gallium nitride (GaN) material in the form of nanowires with catalyst-free, nitrogen-plasma-assisted molecular beam epitaxy (PAMBE) can produce a strain-free crystalline material with a very low defect density in a morphology potentially useful for optoelectronic applications such as nanoscale light emitting diodes and lasers.[1,2,3,4,5] Steady-state photoluminescence (PL) and time-resolved photoluminescence (TRPL) measurements on these nanowires have revealed characteristics of a high-quality, low-defect material.[2,6] Here, we report the results of intensity- and temperature-dependent TRPL measurements and optically pumped lasing behavior for individual *c*-axis, n-type, silicon-doped GaN nanowires grown on Si(111) substrates by PAMBE. It is shown that the PL lifetimes increase with excitation fluence, indicating that nonradiative decay channels are progressively being filled with an increasing number of photogenerated carriers. It is also apparent that with sufficient excitation fluence, we can observe predominantly radiative recombination behavior for free excitons within a limited temperature range—above 70 K (a temperature associated with the binding energy of the donor bound exciton, i.e., $k_B T$=6.2 meV)[7] and below 175 K (where nonradiative recombination at the wire surface becomes important even with higher excitation conditions). Such behavior shows that nonradiative recombination cannot be neglected even at low temperatures, and internal quantum efficiency (IQE) is dependent on the injection level. Lasing threshold measurements on optically pumped nanowires by use of quasisteady-state excitation well above the Mott density reveal lower lasing thresholds at temperatures where radiative excitonic recombination is strong. These measurements reveal the persistence of excitonic recombination behavior in this electron-hole plasma regime.

Steady-state and time-integrated PL top

Nanowires were grown on Si(111) substrates by PAMBE with elemental Ga and Al sources. An AlN buffer layer of 50 nm to 100 nm preceded GaN growth and ultimate spontaneous nanowire formation along the polar *c*-axis direction. The nanowires for this study were n-type, silicon-doped nanowires from a single growth run (designated as B982) with lengths of 10 μm to 22 μm and diameters of 245 nm to 1200 nm. These wire diameters are much greater than the exciton Bohr radius for GaN (~ 3 nm), and no quantum confinement effects are expected.[8,9] The GaN material is well described by a bulk or three-dimensional (3D)

density of states. Doping concentrations N_D were 4×10^{17} to 13×10^{17} cm^{-3}, as determined by resistance and photoconductivity measurements.[10,11]

Steady-state and time-integrated PL measurements on the PAMBE-grown nanowires reveal excitonic spectral peaks of high-quality GaN material. These PL measurements are performed in transmission—the sample is excited on one side, and PL is collected from the opposite side.[2,6] The spectral resolution for these measurements is 0.2 nm, or just under 2 meV at 360 nm. At base temperatures ($T \sim 3$ K), the PL spectrum is dominated by the donor-bound *A*-exciton (D^0X_A) peak. Steady-state PL spectra obtained with a continuous-wave HeCd laser excitation source operating above bandgap at 325 nm (3.815 eV) and time-integrated PL spectra obtained with a frequency-tripled, mode-locked Ti:Sapphire (FTMLTS) laser excitation source operating at 266 nm (4.66 eV) exhibit matching spectral peak positions and linewidths. The strain-free D^0X_A peak at $T \sim 3$ K, for example, is centered at 3.472 eV, with measured linewidths as small as 4 meV full width at half maximum (FWHM). A schematic of the PL/TRPL setup is shown in Fig. 1.

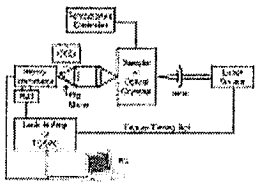

Fig 1.

Schematic of the PL/TRPL measurement setup. Steady-state PL measurements are performed with a continuous-wave HeCd laser source (325 nm) and phase-sensitive detection by use of a lock-in amplifier. TRPL measurements are performed with a FTMLTS source (266 nm) and time-correlated single-photon counting (TCSPC) electronics. A frequency- quadrupled, Q-switched Nd:YVO_4 laser serves as a pump source for the nanowire laser studies. PMT, photomultiplier tube; CCD, charge-coupled device camera for imaging; PC, personal computer.

View first occurrence of Fig. 1 in article.

Figure 2 shows PL spectra at $T \sim 3$ K for n-type, silicon-doped GaN nanowires from the B982 growth run. The solid line is the PL spectrum of as-grown nanowires obtained by exciting nanowires at the edge of a sample piece cleaved from the Si(111) growth substrate. The piece was mounted at ~ 45° so that the excitation beam predominantly (but not exclusively) intercepted protruding nanowires at the sample's edge. This PL spectrum shows the dominant PL peak associated with the D^0X_A. It is at the strain-free position of 3.472 eV and has a measured linewidth of 7 meV (FWHM). At 3.477 eV and 3.482 eV, on the high-energy shoulder of the D^0X_A peak, we see weak evidence of emission from the free *A* exciton (X_A) and free *B* exciton (X_B) resonances, respectively. These are more evident when the PL spectrum is plotted on a linear scale. At 3.455 eV, on the low-energy shoulder of the D^0X_A peak, we see a peak that has been associated with two electron satellites.[12] Also evident is a broader peak at 3.41 eV. This peak is associated with interface defects and stacking faults,[13] which are expected in the defective matrix layer that exists at the base of the as-grown nanowires for this growth run.[14,15] Finally, we see evidence of the first two phonon replicas of the donor-bound exciton peak at 3.38 eV and 3.29 eV, separated from each other and the D^0X_A peak by ~ 92 meV, the LO phonon energy.[16] The first phonon replica appears as a shoulder on the 3.41 eV peak.

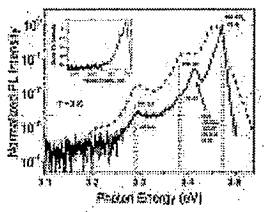

Fig 2.

Photoluminescence spectra of as-grown GaN nanowires (solid line) and of a single GaN nanowire dispersed onto a fused silica substrate (dashed line). $T = 3$ K. The vertical dashed lines indicate the expected strain-free positions of the free A exciton (X_A) and the donor-bound exciton (D^0X_A) lines and their first two phonon replicas (FE-LO, DBE-LO, FE-2LO, DBE-2LO). Inset: the PL spectrum of the dispersed nanowire over an extended range of photon energies (down to 1.8 eV).

View first occurrence of Fig. 2 in article.

To obtain PL spectra from individual nanowires, we typically disperse the nanowires onto a transparent substrate.[2,6] Figure 3 shows field-emission scanning electron microscopy (FESEM) images of a typical nanowire from the B982 growth run under two magnifications. This nanowire has a length of 15 μm and an average diameter of 284 nm. As seen in Fig. 3b, the nanowire exhibits the hexagonal faceting expected for wurtzite GaN. The dispersal and the cooling of the nanowire bound fast to the substrate by van der Waals forces lead to a net tensile strain in the nanowire that has been described previously.[6]

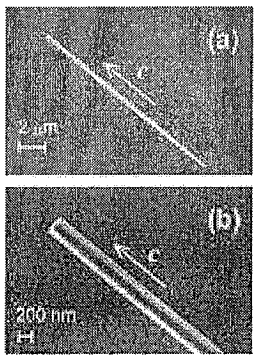

Fig 3.

FESEM images of a typical n-type GaN nanowire from the B982 growth run after dispersal onto a transparent substrate. (a) Image of entire nanowire (15 μm in length). (b) Image of top end of same nanowire (average diameter of 284 nm). The arrows indicate the positive polar c-axis and growth directions. The dispersal substrate here is indium-tin-oxide-coated fused silica.

View first occurrence of Fig. 3b in article.

The dashed line in Fig. 2 shows the PL spectrum of a single nanowire dispersed onto a fused silica substrate. The collected PL signal is stronger here with a better signal-to-noise ratio, because no opaque substrate blocks the collected PL. The PL peak is red shifted by 16 meV and broadened to 27 meV (FWHM). The redshift matches the peak shift expected for a cooled wire under tensile strain on a fused silica substrate.[6] The peak broadening is probably indicative of a strain gradient introduced with the dispersal.[6,17] Three phonon replicas are easily discernable in the PL spectrum of the dispersed nanowire, with peak positions of 3.39 eV, 3.29 eV, and 3.20 eV (all ±0.01 eV; separations are 100 and 90 ± 10 meV, respectively). The separation of the first phonon replica from the D^0X_A peak is 60 ± 10 meV, well below the energy of an LO phonon. This suggests a stronger role of the phonon replicas of the free excitons (X_A and X_B) in the PL spectrum of the strained nanowire. Similar enhancement of free-exciton phonon replica peaks has been observed in strained ZnO nanowires when compared to unstrained nanowires.[6,17] However, the positions of the phonon replicas in these strained GaN nanowires is not fully understood and requires more study. Finally, no peak at 3.41 eV is visible, indicating that the dispersed nanowire is free of material from the defective matrix layer.

The inset of Fig. 2 shows the PL spectrum of the dispersed nanowire over an extended range of photon energies (down to 1.8 eV). No evidence of yellow luminescence, which is associated with material defects and possible carbon contamination,[12,18] is observed.

The peak broadening observed in the PL spectra of the dispersed nanowires obscures the spectrally distinct excitonic resonances, and for convenience, we simply report TRPL measurements at wavelengths of peak luminescence for each temperature in the results below.

Time-resolved PL versus injection level and temperature top

The PL lifetimes were obtained by use of the FTMLTS laser pump source. This source excited a nanowire sample within an evacuated, continuous-flow helium cryostat with optical access ports. Collected PL light was dispersed through a monochromator and fell onto a fast multichannel plate photomultiplier tube (PMT). Time-correlated single-photon counting electronics were used to build a histogram giving the temporal response measurements (see Fig. 1).[6] The temporal resolution of this system was below 50 ps. The excitation pulses were ~ 150 fs in duration (FWHM) with a repetition rate of 2 MHz. Pulse fluence at the nanowire sample ranged from 25 μJ/cm^2 to 190 μJ/cm^2. This gives a photogenerated excess carrier density Δp of $\Delta p = 0.7 - 47 \times 10^{18}$ cm^{-3} for the transient conditions of this pump (see Appendix). The TRPL decay data were fitted to a single exponential decay function with the method of least squares to obtain the PL lifetimes. Computer control enabled more rapid collection of multiple TRPL traces. Figure 4 shows the temporal evolution of the PL spectrum for a dispersed nanowire with a ~ 460 nm diameter and a 15.1 μm length at $T \sim 3$ K. This was obtained by recording multiple TRPL traces at different PL wavelengths. The upper inset of Fig. 4 shows an example TRPL trace taken at 3.45 eV (359 nm). Data appear as open squares. The solid line represents the best fit for a single exponential decay. The lower inset shows a FESEM image of the nanowire on the dispersal substrate.

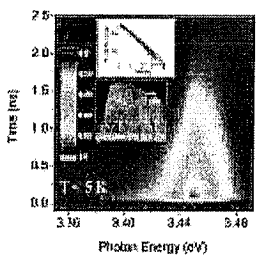

Fig 4.

(Color online) Temporal evolution of the PL spectrum for a dispersed n-type GaN nanowire with a diameter of ~460 nm and a length of 15.1 μm at $T \approx 3$ K. The pump source for this measurement is a frequency-tripled mode-locked Ti:Sapphire laser. The scale bar indicates the normalized PL intensity. The upper inset shows an example TRPL trace taken at a PL emission wavelength of 359 nm (3.45 eV); the solid line represents the best fit for a single exponential decay. The lower inset is a FESEM image of the dispersed nanowire (oriented vertically in the image).

View first occurrence of Fig. 4 in article.

The PL lifetimes varied with excitation fluence and temperature. Figure 5 shows the PL lifetimes as a function of excitation pulse fluence for the same dispersed nanowire pictured in Fig. 4 at a temperature of $T = 100$ K. Evidence of saturation in the PL lifetimes occurs below the maximum pulse fluence obtainable from the FTMLTS laser source (190 μJ/cm^2). A look at the temperature-dependent PL lifetimes (Fig. 6) shows an increase in the slope of PL lifetime versus temperature for higher excitation pulse fluences. This occurs within a temperature range of 70 K to 175 K. Figure 6 shows the temperature dependence of the PL lifetimes for an excitation pulse fluence of 25 μJ/cm^2 (triangles) and an excitation pulse fluence of 190 μJ/cm^2 (squares). A comparison with the theory of Dmitriev and Oruzheinikov (Ref. 9) shows that with sufficient excitation, the measured PL lifetimes here are close to the expected radiative lifetimes of free excitons in bulk GaN. The expected temperature-dependent radiative lifetimes of these free excitons are given by

$$\tau_{X,\mathrm{rad}} = KT^{3/2}, \qquad (1)$$

where the coefficient for GaN is calculated to be $K = 0.73$ ps/K$^{3/2}$ (Ref. 9). At a temperature of $T \sim 70$ K, the X_A peak overcomes

the D^0X_A peak in the PL spectrum, and free-exciton recombination behavior is expected. Sufficient excitation is required to saturate the nonradiative recombination channels associated with the surface states in this otherwise near-defect-free nanowire. The ~ $T^{3/2}$ dependence reflects the fact that the free excitons more effectively populate the 3D density of states with increasing temperature, and, as a result, fewer excitons have a low enough center-of-mass kinetic energy to radiatively recombine.[19]

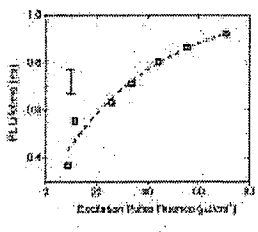

Fig 5.

PL lifetimes vs excitation fluence for the same dispersed GaN nanowire pictured in Fig. 2 at a temperature of T ≈ 100 K. The dotted line serves as a guide for the eye. The error bar represents the uncertainty in the measurements of the lifetimes.

View first occurrence of Fig. 5 in article.

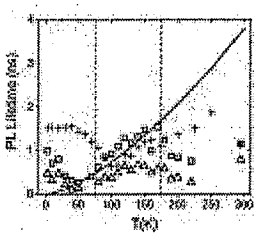

Fig 6.

Temperature-dependent PL lifetimes from single-exponential fits for two nanowire excitation fluences—190 microJoules/cm^2 (squares) and 25 microJoules/cm^2 (triangles)—and PL lifetimes (excluding subnanosecond transients) for a free-standing HVPE-grown bulk GaN sample (crosses) at an excitation fluence of ~20 μJ/cm^2. The solid line represents the expected radiative lifetimes of free excitons in bulk GaN as per Ref. 9. The size of the symbols represents the uncertainty associated with the measurements of the PL lifetimes. The vertical dashed lines bound the region where radiative recombination is dominant at the higher nanowire excitation fluence.

View first occurrence of Fig. 6 in article.

As mentioned above (and as calculated in the Appendix), the higher pulse fluences of the ultrafast FTMLTS source can briefly produce high carrier densities ($\Delta p = 47 \times 10^{18}$ cm^{-3}), which are well above the Mott density where excitons give way to an electron-hole plasma (EHP).[20] From measurements of the dielectric function via spectroscopic ellipsometry (SE) on n-type GaN with different doping concentrations, Shokovets et al. (Ref. 21) calculate a room temperature Mott density, n_M, of 3×10^{18} cm^{-3}, and from quasisteady-state PL measurements of n-type GaN under intense excitation conditions, Binet et al. calculate a room-temperature Mott density of $n_M = 10 \times 10^{18}$ cm^{-3} (Refs. 20,21). Although the calculations based on SE measurements use a more traditional criterion to obtain n_M (i.e., one based on the relation between the dielectric screening length and the exciton Bohr radius, $a_x \sim 3$ nm in GaN [Ref. 8]), the results of Binet et al.[20] illustrate that excitonic effects play an important role at significantly higher carrier densities. In addition, Shokovets et al.[21] indicate that the Coulomb interaction between conduction-band electrons and valence-band holes that is responsible for exciton formation continues to enhance optical transitions above the Mott density. This is especially true for GaN excited well above the bandgap, as is true in our measurements. Above-bandgap pumping creates electron-hole pairs with finite kinetic energies ($E_{\text{exc photon}} - E_g$, where E_g is the bandgap energy) that are less susceptible to the effects of screening.[21] Finally, at $T = 150$ K, the PL intensity, I_{PL}, is nearly proportional to the pulse excitation fluence, F_{exc}. That is, a least-squares fit of the I_{PL} vs F_{exc} data yields a power-law exponent γ of ~ 1.3 for the relation

$$I_{PL} \propto F_{exc}^{\gamma}, \qquad (2)$$

where $\gamma = 1$ indicates purely excitonic recombination, $\gamma = 2$ indicates purely free-carrier recombination, and $1 < \gamma < 2$ indicates an intermediate case with both excitonic and free-carrier recombination.[22,23] For these reasons, we believe that under the transient pump conditions of our experiments and within a temperature range of 75 K < T < 175 K, the PL decay observed in our TRPL measurements is almost exclusively due to the enhanced radiative recombination of free excitons. That is, the temperature-dependent PL decay should match the results of Dmitriev and Oruzheinikov[9] as plotted in Fig. 6, and in this temperature range, the IQE is near unity.

The IQE did not approach unity for more defective GaN material. Similar temperature-dependent TRPL data taken from the defective matrix material of the same B982 growth run (described above) exhibits no clear ~ $T^{3/2}$ temperature dependence or radiative decay behavior. The additional nonradiative recombination channels associated with the increased defect density gave shortened PL lifetimes that masked the radiative recombination trends seen with the low-defect GaN nanowire.

Below ~ 70 K, the monitored peak luminescence is primarily due to recombination of the donor-bound exciton, D^0X_A. The temperature-dependent PL lifetimes are well described by the thermally activated nonradiative recombination associated with the disassociation of the donor-bound exciton into a free exciton and an isolated donor. Pozina et al.[7] arrive at the following expression for PL lifetime, τ_{PL}:

$$\frac{1}{\tau_{PL}} = \frac{1}{\tau_{rad,0}} + A\exp\left(\frac{-E_a}{kT}\right), \qquad (3)$$

where E_a is the activation energy, $\tau_{rad,0}$ is the radiative lifetime at $T = 0$ K, and A is a temperature-independent recombination rate. A best fit of Eq. (1) to the 190 μJ/cm² data of Fig. 4 yields $\tau_{rad,0} = 870$ ps and an activation energy E_a of 8 meV, which is close to the localization energy of D^0X_A and similar to the results of Pozina et al.[7,24]

Above $T = 175$ K, PL lifetimes deviate from what is expected for radiative excitonic decay. At these temperatures, nonradiative surface recombination is not saturated even at the maximum pulse fluences produced by the FTMLTS laser pump. The expected free-exciton radiative lifetime $\tau_{x,rad}$ given by Eq. (1) and indicated by the solid line in Fig. 6 is 3.8 ns at room temperature. The free-exciton radiative lifetime $\tau_{x,rad}$ is associated with an enhanced radiative recombination rate. The lifetime of free-carrier radiative recombination,

$$\tau_{rad} = \frac{1}{B(T)N_D}, \qquad (4)$$

where $B(T)$ is the radiative recombination coefficient, is expected to be 1 order of magnitude longer. For the estimated doping concentrations N_D of our n-type B982 nanowires, $\tau_{rad} \sim 23$ ns at $T = 200$ K, and $\tau_{rad} \sim 38$ ns at $T = 295$ K.[9] At room temperature, the thermal energy of the lattice, $k_BT = 25.4$ meV, exceeds the binding energy of the exciton (20.4 ± 0.5 meV),[25] and with the transient pumping of our FTMLTS laser source, the carrier temperatures can briefly be higher still.[26] Both exciton and free-carrier recombination are expected to coexist. Indeed, measurements of I_{PL} vs F_{exc} reveal that the exponent γ of Eq. (2) increases to 1.5 ± 0.1 at room temperature, indicating a relatively stronger role for free-carrier recombination.[23] A good estimate of the room-temperature IQE for free-exciton recombination in this nanowire can be calculated as[8]

$$IQE_X\left(T\right) = \frac{\tau_{nr}(T)}{\tau_{x,rad}(T) + \tau_{nr}(T)}, \qquad (5)$$

where

$$\tau_{nr} = \left(\frac{1}{\tau_{PL}} - \frac{1}{\tau_{x,rad}}\right)^{-1}. \qquad (6)$$

Based on the τ_{PL} data in Fig. 4, $IQE_X(T = 295\text{ K}) = 30\%$ at an excitation fluence of 190 μJ/cm², and $IQE_X(T = 295\text{ K}) = 21\%$ at an excitation fluence of 25 μJ/cm², where the nonradiative decay is due to recombination at the surface.[6] For free-carrier

recombination, a similar calculation (replacing $\tau_{x,rad}$ with τ_{rad}) yields $IQE_{EHP}(T=295\ K)=3\%$ and 2% for the 25 μJ/cm² and 190 μJ/cm² excitation fluences, respectively. In summary,

$$3\% \leq IQE(T=295\ K) \leq 30\% \qquad (7)$$

at an excitation fluence of 190 μJ/cm². Given similar contributions from excitonic and free-carrier recombination as suggested by the room-temperature value of γ, the overall IQE was roughly 15%.

Although the relationship is understood by many,[27] it is important to emphasize that IQE (as shown here) is strongly dependent on excitation carrier density and should be measured under conditions matching those of the desired application. The IQE at high injection levels associated with a laser diode, for example, will in general be different from that at the lower injection levels associated with a light emitting diode. The persistent practice of assuming unity IQE at low temperatures regardless of injection level can lead to erroneous results. For example, temperature-dependent measurements of integrated PL intensity, I_{PL}, on the B982 nanowire shown in Fig. 2 by use of the HeCd laser pump (325 nm, 7.8 kW/cm²) give apparent (IQE = [I_{PL}(T = 250 K)]/[I_{PL}(T_{cold})]) (Ref. 8) values of greater than 60% with the temperature $T_{cold}=5$ K, and greater than 80% with $T_{cold}=$ 100 K, close to the coldest free-exciton temperature. (Here, the integrated PL intensity is obtained by reducing the spectral resolution of the measurement from 0.2 nm to 0.5 nm by widening the entrance and exit slits of the monochromator.) These misleading results stem from the incorrect assumption that at low temperatures one has purely radiative decay. This is not the case for the excitation levels of our HeCd pump.

Finally, for comparison, Fig. 6 also includes PL lifetime data acquired from a high-quality piece of free-standing bulk GaN grown by hydride-vapor-phase-epitaxy (HVPE). For this sample, PL was collected from the side of the sample that faced the laser source, with the aid of a beam splitter. That is, the laser source, the collection optics, the monochromator, and the PMT were moved to the right of the sample and the cryostat, as shown in Fig. 1. The x-ray and PL measurements from this sample have been reported previously.[28] Unlike the nanowire TRPL traces (e.g., see the inset of Fig. 4), the TRPL traces obtained from this 250 μm thick sample exhibited leave nonsingle as is nonsingle-exponential decays. The traces consisted of subnanosecond transients followed by a slower decay component. The fast transients are associated with the redistribution of the photo-generated carriers into the bulk and away from the limited region where PL is collected. This process was described by Malinauskas et al. in their study of nonequilibrium carrier dynamics in freestanding GaN.[29] The PL decay times for the HVPE GaN plotted in Fig. 6 are the slower decay components determined from multiexponential fits to the decay data. Like the nanowire data, these temperature-dependent decay times are close to those expected for purely radiative excitonic recombination [Eq. (1)] in the temperature range of $T\sim$ 100–175 K. Below 100 K, a drop in PL lifetime is observed as the donor-bound exciton disassociates with increasing temperature. Above 175 K and below room temperature, the HVPE GaN decay times drop below those expected for purely radiative excitonic recombination, but they exceed those of the nanowires, which suffer more from nonradiative recombination at the surfaces. However, at $T=294$ K, the decay times for the nanowire and the bulk GaN are nearly identical, yielding matching room-temperature IQEs.

Optically pumped nanowire lasers top

As demonstrated in other nanowires,[30,31] with sufficient optical pumping, our PAMBE-grown GaN nanowires produce stimulated as well as laser emission. Laser emission was not detected with the transient pumping provided by the FTMLTS laser. With extremely short, delta-function (~150 fs FWHM) excitation pulses, the FTMLTS laser most likely produces gain-switched lasing pulses from the nanowire with durations that depend on the photon lifetime of the laser cavity and the differential gain coefficient of GaN.[32,33] Based on parameters typical of our nanowires, these gain-switched pulses are expected to have durations below a few picoseconds, too short to be observed with our current TRPL and PL measurement setups. In addition, the diameters of the excitation spots used in the TRPL measurements were typically shorter than the

nanowire lengths. Portions of the nanowire would be strongly absorbing under these conditions, increasing the laser threshold substantially. However, lasing was observed with a frequency-quadrupled Q-switched Nd:YVO_4 laser pump. This 266 nm pump produced pulses with 8 ns FWHM durations at a repetition rate of 15 kHz and average output powers up to 8.5 mW. The 8 ns pulse duration is several multiples of the GaN minority carrier lifetime (~ 1 ns), and thus steady-state conditions are achieved within the duration of an excitation pulse. The lasing thresholds of 21 separately dispersed GaN nanowires from the same B982 growth run were measured. Peak power intensities at the sample were kept below 10 MW/cm^2 to avoid nanowire and substrate damage, and the beam spot encompassed the entire nanowire. The dimensions and morphology of each dispersed wire were determined via FESEM. Wire lengths ranged from 10.5 μm to 18.7 μm. The wires had varying degrees of taper and different end qualities. With diameters of greater than 200 nm and a material index of refraction of ~ 2.7, these GaN nanowires are multimode waveguides with strong confinement that can support over 20 transverse modes.[34] The lasing threshold was not a strong function of the nanowire diameter; it depended more on wire morphology and wire-end quality. The threshold peak intensities varied from 200 kW/cm^2 up to 3.26 MW/cm^2. The lasing spectra typically exhibited multiple lines corresponding to the oscillation of multiple axial modes. The axial mode separations ranged from 0.53 nm to 1.2 nm and were related to the round trip optical path lengths of these highly dispersive nanowire laser cavities.[35] The room-temperature lasing spectra from a single optically pumped nanowire at different pump intensities are shown in Fig. 7. This nanowire was 12.4 μm long and 245 nm in diameter, with flat ends and no measurable taper. The inset in Fig. 7 shows the laser emission intensity versus the pump intensity. This wire had a threshold pump intensity of 225 kW/cm^2. Nanowires with good morphology (low taper) and flat ends were essential for low-threshold laser operation. The lasing threshold intensity for a second B982 nanowire (13.6 μm long and ~ 350 nm diameter with a 75 nm taper) is plotted as a function of temperature in Fig. 8. The lasing threshold intensities were lowest at temperatures where excitonic radiative recombination was shown to be strong, that is, where nonradiative recombination played a minor role. This is despite the fact that the quadrupled Nd:YVO_4 pump produced a *sustained* fluence of greater than 1 mJ/cm^2, corresponding to an excess carrier density of Δp [mt] 2×10^{19} cm^{-3}, i.e., well above the Mott density.

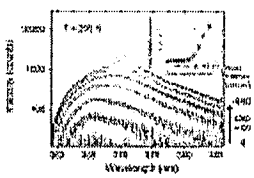

Fig 7.

(Color online) Room-temperature luminescence and lasing spectra from a dispersed n-type GaN nanowire pumped at 7 different peak pump intensities from a frequency-quadrupled, Q-switched Nd:YVO_4 laser source. The n-type GaN nanowire was 12.4 μm long and 245 nm in diameter with flat ends and no measurable taper. The inset shows the peak nanowire emission intensity vs the pump intensity. The lasing threshold for this optically pumped nanowire is 225 kW/cm^2.

View first occurrence of Fig. 7 in article.

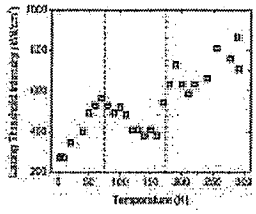

Fig 8.

Temperature-dependent lasing threshold intensities for a dispersed n-type GaN nanowire with an average diameter of 350 nm, length of 13.6 mm, and taper of 75 nm. The pump source here is a frequency-quadrupled Q-switched Nd:YVO_4 laser. Lasing threshold intensities are lower where excitonic radiative recombination was shown to be strong despite the higher fluence and quasisteady-state nature of the pump source. The vertical dashed lines bound the same temperature range highlighted in Fig. 4.

View first occurrence of Fig. 8 in article.

CONCLUSION top

In conclusion, with sufficient excitation, low-defect GaN nanowires exhibit purely radiative recombination behavior that closely matches that seen in high-quality bulk GaN yet which is absent in more defective material. Injection-level-dependent TRPL and PL measurements made at different temperatures on low-defect nanowires revealed near-unity IQE around $T \sim 120$ K and an effective IQE of ~15% at room temperature, given a FTMLTS laser pump. Free excitons played the dominant role in the radiative recombination from ~75 K up to ~175 K. At room temperature, the strong nonradiative recombination was due to recombination at the surface. Temperature-dependent measurements of lasing thresholds in optically pumped nanowires showed a strong dependence on wire morphology, with lower thresholds at temperatures where radiative excitonic recombination was demonstrated to be strong with a lower-fluence ultrafast pump.

ACKNOWLEDGMENTS

We thank Adam Cole and Nancy Haegel of the Naval Postgraduate School for their measurement of minority carrier diffusion length in an isolated, n-type, PAMBE-grown, GaN nanowire.

APPENDIX: Estimated excess carrier density for TRPL measurements

The excess carrier density Δp can be estimated as

$$\Delta p = \frac{F}{h\nu}\alpha_{\text{eff}}, \qquad \text{(A1)}$$

where F is the excitation pulse fluence (25 μJ/cm^2 to 190 μJ/cm^2), $h\nu$ is the excitation photon energy (7.47×10^{-19} J or 4.66 eV), and α_{eff} is the effective absorption coefficient. For our experimental conditions, α_{eff} lies between the optical absorption coefficient α_{opt} ($= 1.8 \times 10^5$ cm^{-1} at 4.66 eV, room temperature)[25] and the reciprocal of the nanowire diameter φ_{NW}.[20] That is,

$$\frac{1}{\Phi_{\text{NW}}} < \alpha_{\text{eff}} < \alpha_{\text{opt}}. \qquad \text{(A2)}$$

This is because the carriers initially generated within the optical penetration depth ($1/\alpha_{\text{opt}} = 56$ nm) eventually diffuse to the opposite side of the nanowire, given a minority-carrier diffusion length L_D that exceeds this diameter.

The minority carrier (hole) diffusion length $L_D = \sqrt{D\tau}$ for our n-type GaN nanowires has been estimated from near-field optical microscopy measurements to be $L_D \sim 500$ nm,[36] which exceeds φ_{NW}. Here D is the diffusion coefficient and $\tau \sim 1$ ns is the minority carrier lifetime. With the ultrafast (150 fs FWHM) pulse excitation provided by the FTMLTS laser source, the excess carrier density falls with time as the photogenerated carriers diffuse a length L_D in a time span of the minority carrier lifetime τ, or the carriers traverse the wire diameter of ~ 460 nm in less than 1 ns. Eq. ((1)) gives the quoted range for Δp under these

transient conditions. These values represent an upper bound because carrier capture by the nonradiative centers and lateral diffusion along the wire axis have been neglected.

1. E. Calleja, M. Sanchez-Garcia, F. Sanchez, F. Calle, F. Naranjo, E. Munoz, U. Jahn, and K. Ploog, Phys. Rev. B **62**, 16826 (2000). | first citation in article

2. J. Schlager, N. Sanford, K. Bertness, J. Barker, A. Roshko, and P. Blanchard, Appl. Phys. Lett. **88**, 213106 (2006). | first citation in article

3. K. Bertness, J. Schlager, N. Sanford, A. Roshko, T. Harvey, and A. Davydov, in *GaN, AlN, InN and Related Materials* (Materials Research Society, Warrendale, PA, 2006), p. 799. | first citation in article

4. H. Sekiguchi, K. Kishino, and A. Kikuchi, Appl. Phys. Lett. **96**, 231104 (2010). | first citation in article

5. O. Brandt, C. Pfuller, C. Cheze, L. Geelhaar, and H. Riechert, Phys. Rev. B **81**(4), 045302 (2010). | first citation in article

6. J. Schlager, K. Bertness, P. Blanchard, L. Robins, A. Roshko, and N. Sanford, J. Appl. Phys. **103**, 124309 (2008). | first citation in article

7. G. Pozina, J. Bergman, T. Paskova, and B. Monemar, Appl. Phys. Lett. **75**, 4124 (1999). [ISI] | first citation in article

8. S. Nakamura and S. F. Chichibu, *Introduction to Nitride Semiconductor Blue Lasers and Light Emitting Diodes* (Taylor & Francis, London, 2000). | first citation in article

9. A. Dmitriev and A. Oruzheinikov, J. Appl. Phys. **86**, 3241 (1999). [ISI] | first citation in article

10. L. Mansfield, K. Bertness, P. Blanchard, T. Harvey, A. Sanders, and N. Sanford, J. Electron. Mater. **38**, 495 (2009). | first citation in article

11. N. Sanford, P. Blanchard, K. Bertness, L. Mansfield, J. Schlager, A. Sanders, A. Roshko, B. Burton, and S. George, J. Appl. Phys. **107**, 034318 (2010). | first citation in article

12. M. Reshchikov and H. Morkoc, J. Appl. Phys. **97**, 061301 (2005). | first citation in article

13. F. Furtmayr, M. Vielemeyer, M. Stutzmann, A. Laufer, B. Meyer, and M. Eickhoff, J. Appl. Phys. **104**, 074309 (2008). | first citation in article

14. K. A. Bertness, A. Roshko, N. A. Sanford, J. M. Barker, and A. Davydov, J. Cryst. Growth **287**, 522 (2006). [Inspec] | first citation in article

15. K. Bertness, A. Roshko, L. Mansfield, T. Harvey, and N. Sanford, J. Cryst. Growth **310**, 3154 (2008). | first citation in article

16. V. Davydov, Y. Kitaev, I. Goncharuk, A. Smirnov, J. Graul, O. Semchinova, D. Uffmann, M. Smirnov, A. Mirgorodsky, and R. Evarestov, Phys. Rev. B **58**, 12899 (1998). | first citation in article

17. L. Robins, K. Bertness, J. Barker, N. Sanford, and J. Schlager, J. Appl. Phys. **101**, 113505 (2007). | first citation in article

18. G. T. Wang, A. A. Talin, D. J. Werder, J. R. Creighton, E. Lai, R. J. Anderson, and I. Arslan, Nanotechnology **17**, 5773 (2006). | first citation in article

19. J. Im, A. Moritz, F. Steuber, V. Harle, F. Scholz, and A. Hangleiter, Appl. Phys. Lett. **70**, 631 (1997). | first citation in

article

20. F. Binet, J. Duboz, J. Off, and F. Scholz, Phys. Rev. B **60**, 4715 (1999). | first citation in article

21. S. Shokhovets, K. Kohler, O. Ambacher, and G. Gobsch, Phys. Rev. B **79**(4), 045201 (2009). | first citation in article

22. J. Fouquet and A. Siegman, Appl. Phys. Lett. **46**, 280 (1985). | first citation in article

23. X. Chen, J. Huso, J. Morrison, and L. Bergman, J. Appl. Phys. **99**, 046105 (2006). | first citation in article

24. G. Pozina, C. Hemmingsson, J. Bergman, D. Trinh, L. Hultman, and B. Monemar, Appl. Phys. Lett. **90**, 221904 (2007). [ISI] | first citation in article

25. J. Muth, J. Lee, I. Shmagin, R. Kolbas, H. Casey, B. Keller, U. Mishra, and S. DenBaars, Appl. Phys. Lett. **71**, 2572 (1997). | first citation in article

26. S. Jursenas, N. Kurilcik, G. Kurilcik, A. Zukauskas, P. Prystawko, M. Leszcynski, T. Suski, P. Perlin, I. Grzegory, and S. Porowski, Appl. Phys. Lett. **78**, 3776 (2001). | first citation in article

27. S. Watanabe, N. Yamada, M. Nagashima, Y. Ueki, C. Sasaki, Y. Yamada, T. Taguchi, K. Tadatomo, H. Okagawa, and H. Kudo, Appl. Phys. Lett. **83**, 4906 (2003). | first citation in article

28. K. Bertness, N. Sanford, J. Barker, J. Schlager, A. Roshko, A. Davydov, and I. Levin, J. Electron. Mater. **35**, 576 (2006). [Inspec] | first citation in article

29. T. Malinauskas, K. Jarasiunas, S. Miasojedovas, S. Jursenas, B. Beaumont, and P. Gibart, Appl. Phys. Lett. **88**, 202109 (2006). | first citation in article

30. M. Zimmler, F. Capasso, S. Muller, and C. Ronning, Semicond. Sci. Technol. **25**, 024001 (2010). | first citation in article

31. S. Gradecak, F. Qian, Y. Li, H. Park, and C. Lieber, Appl. Phys. Lett. **87**, 173111 (2005). | first citation in article

32. P. Vasil'ev, *Ultrafast Diode Lasers: Fundamentals and Applications* (Artech House, Boston, 1995). | first citation in article

33. Y. Arakawa, T. Sogawa, M. Nishioka, M. Tanaka, and H. Sakaki, Appl. Phys. Lett. **51**, 1295 (1987). [ISI] | first citation in article

34. A. Maslov and C. Ning, Appl. Phys. Lett. **83**, 1237 (2003). | first citation in article

35. A. E. Siegman, *Lasers* (University Science Books, Mill Valey, CA, 1986). | first citation in article

36. L. Baird, G. Ang, C. Low, N. Haegel, A. Talin, Q. Li, and G. Wang, Physica B **404**, 4933 (2009). | first citation in article

---

Erratum: "Photoluminescence of Mg-ion implantation in low-temperature grown GaAs" [J. Appl. Phys. 75, 2628 (1994)]
J. Appl. Phys. **76**, 2563 (1994)

Erratum: "Photoluminescence study of impurity states in aluminum antimonide" [J. Appl. Phys. 67, 1478 (1990)]
J. Appl. Phys. **68**, 1944 (1990)

Comment on "Nanoscale InP islands embedded in InGaP" [Appl. Phys. Lett. 66, 361 (1995)]
Appl. Phys. Lett. **67**, 1166 (1995)

Photoluminescence from narrow InAs-AlSb quantum wells
Appl. Phys. Lett. **62**, 3303 (1993)

Optical properties of quantum wells grown upon gas source molecular-beam epitaxy low-temperature buffers
J. Appl. Phys. **69**, 7942 (1991)

Excitonic luminescence and absorption in dilute GaAs1−xNx alloy (x<0.3%)
Appl. Phys. Lett. **70**, 2984 (1997)

Erratum: "Effects of insertion of strain-mediating layers on luminescence properties of 1.3-μm GaInNAs/GaNAs/GaAs quantum-well structures" [Appl. Phys. Lett. 80, 3054 (2002)]
Appl. Phys. Lett. **80**, 4872 (2002)

Nature of compensating luminescence centers in Te-diffused and -doped GaSb
J. Appl. Phys. **80**, 1112 (1996)

Growth and characterization of AlInGaN quaternary alloys
Appl. Phys. Lett. **68**, 40 (1996)

High-pressure photoluminescence study of ordered Ga0.5In0.5P alloys grown on GaAs by organometallic vapor phase epitaxy
Appl. Phys. Lett. **58**, 1289 (1991)

Photoluminescence and photoreflectance from GaAs/AlAs multiple quantum wells
J. Appl. Phys. **78**, 3376 (1995)

Anomalous PL Brightening Inside A Current Density Filament In n-GaAs Under A Pulsed Electric Field
AIP Conf. Proc. **893**, 127 (2007)

Photoluminescence excitation measurements on GaAs:Er grown by molecular-beam epitaxy
J. Appl. Phys. **61**, 4877 (1987)

Observation of photoluminescence from Al1−xInxN heteroepitaxial films grown by metalorganic vapor phase epitaxy
Appl. Phys. Lett. **73**, 830 (1998)

Photoluminescence study on undoped single quantum well pseudomorphic structures
Appl. Phys. Lett. **53**, 2158 (1988)

Subpicosecond photoluminescence from radiation-damaged Ga0.47In0.53As
Appl. Phys. Lett. **55**, 460 (1989)

Optical spectroscopy of single, site-selected, InAs/InP self-assembled quantum dots
Appl. Phys. Lett. **84**, 978 (2004)

1.3 μm photoluminescence from InGaAs quantum dots on GaAs
Appl. Phys. Lett. **67**, 3795 (1995)

A model for the Fe-related emission at 3057 cm−1 in GaAs
J. Appl. Phys. **71**, 5703 (1992)

Single quantum well photoluminescence in ZnSe/GaAs/AlGaAs grown by migration-enhanced epitaxy
Appl. Phys. Lett. **55**, 1235 (1989)